

# Design of Two-Stage Class AB CMOS Buffers: A Systematic Approach

---

Antonio Lopez Martin, Jose Maria Algueta Miguel, Lucia Acosta,  
Jaime Ramirez-Angulo, and Ram3n Gonzalez Carvajal

**A systematic approach for the design of two-stage class AB CMOS unity-gain buffers is proposed. It is based on the inclusion of a class AB operation to class A Miller amplifier topologies in unity-gain negative feedback by a simple technique that does not modify quiescent currents, supply requirements, noise performance, or static power. Three design examples are fabricated in a 0.5  $\mu\text{m}$  CMOS process. Measurement results show slew rate improvement factors of approximately 100 for the class AB buffers versus their class A counterparts for the same quiescent power consumption ( $< 200 \mu\text{W}$ ).**

**Keywords:** Analog integrated circuits, CMOS buffer, CMOS voltage follower, quasi-floating gate.

## I. Introduction

Class AB buffers are required in low-power analog design and mixed-signal design to drive low impedance loads. In these scenarios, adequate dynamic performance must be compatible with low quiescent power consumption. This requirement is not viable if buffers operate in class A since, in this case, the load current is limited by the quiescent current of the output stage, leading to a tradeoff between slew rate and quiescent power. Class AB implementations solve this design constraint by providing dynamic currents to the load which are not limited by the quiescent currents. Several class AB buffers have been proposed which are mainly based on using a properly biased push-pull output stage [1]-[5]. However, typical shortcomings of these proposals are that the additional circuitry employed to get class AB operation often increases power consumption, decreases current efficiency (defined as the percentage of supply current that is delivered to the load), and sometimes does not feature accurate control of quiescent currents. Another typical shortcoming of some buffers is that there is a DC level shift between the input and the output voltage [6], [7], which is often dependent on temperature and process variations and that can be important if the buffer is used in a single-ended configuration.

In this paper, we propose a technique to systematically derive two-stage class AB unity-gain buffers from class A implementations. The technique is based on the use of quasi-floating gate (QFG) techniques [8]-[11] which allow the inclusion of a class AB operation without requiring additional power consumption or supply voltage and featuring a simple and accurate control of quiescent currents.

The paper is organized as follows. Section II describes the

---

Manuscript received Aug. 3, 2010; revised Oct. 5, 2010; accepted Oct. 25, 2010.

This work was supported by the Spanish Direcci3n General de Investigaci3n and FEDER funds under grant TEC2010-21563-C02.

Antonio Lopez Martin (phone: +34948169311, email: antonio.lopez@unavarra.es) and Jose Maria Algueta Miguel (email: josemaria.algueta@unavarra.es) are with the Department of Electrical and Electronic Engineering, Public University of Navarra, Navarra, Spain.

Lucia Acosta (email: lucia@gte.esi.us.es) and Ram3n Gonzalez Carvajal (email: carvajal@gte.esi.us.es) are with the Department of Electrical and Computer Engineering, University of Seville, Seville, Spain.

Jaime Ramirez-Angulo (email: irez@nmsu.edu) is with the Department of Electrical and Computer Engineering, New Mexico State University, Las Cruces, New Mexico, USA.  
doi:10.4218/etrij.11.0110.0465

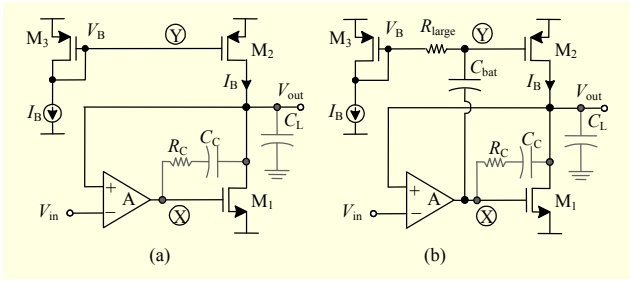


Fig. 1. (a) Class A voltage follower and (b) class AB QFG voltage follower.

systematic approach proposed and three design examples. Measurement results for a test chip prototype containing the three buffers and their class A versions are presented in section III. Finally, conclusions are drawn in section IV.

## II. Systematic Design of Two-Stage Class AB Buffers

Figure 1 illustrates the basic design principle proposed. A generic class A buffer formed by a two-stage Miller amplifier in unity-gain negative feedback and shown in Fig. 1(a) is transformed into the class AB version of Fig. 1(b) by properly including a floating capacitor and a large resistive device, that is, making the gate of  $M_2$  a quasi-floating gate node. Details about the starting and resulting topologies are provided in the next paragraphs.

### 1. Class A Two-Stage Unity-Gain Buffer

Figure 1(a) shows a conventional two-stage class A unity-gain buffer. Amplifier A represents a generic single-stage amplifier with DC gain  $A = G_{mA}R_A$ , where  $G_{mA}$  and  $R_A$  are the transconductance and output resistance of the amplifier. The negative feedback loop formed by the amplifier and transistor  $M_1$  has a high DC loop gain of  $A_{ol} = G_{mA}R_A g_{m1}(r_{o1} || r_{o2})$ , where  $g_{m1}$  and  $r_{o1}$  are the transconductance and output resistance of transistor  $M_1$ , respectively. This high loop gain forces the output voltage to track the input voltage, being the DC closed-loop gain of the buffer:

$$A_{cl} = \frac{V_{out}}{V_{in}} = \frac{A_{ol}}{1 + A_{ol}} \approx 1. \quad (1)$$

Also, due to the action of the feedback loop, the output resistance is very low. It is given by

$$R_{out} = \frac{1}{G_{mA}R_A g_{m1}}. \quad (2)$$

Stability of the feedback loop in Fig. 1(a) is enforced by creating a dominant pole  $f_{p1}$  at node X using Miller compensation by capacitor  $C_C$ . A nulling resistor is often

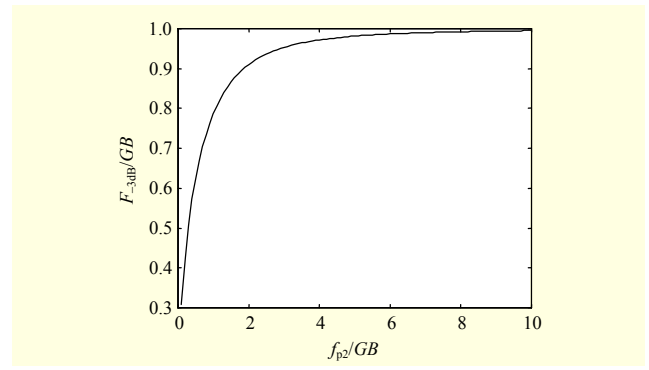


Fig. 2. Graphical representation of (4).

employed, as shown in Fig. 1(a). The non-dominant pole  $f_{p2}$  corresponds to the output node. These poles are:

$$f_{p1} \approx \frac{1}{2\pi R_A g_{m1} (r_{o1} || r_{o2}) C_C}, \quad (3)$$

$$f_{p2} \approx \frac{g_{m1}}{2\pi (C_X + C_L)},$$

where  $C_X \approx C_{GS1}$  is the intrinsic capacitance at node X, yielding a bandwidth for the buffer of approximately

$$f_{-3dB} \approx \frac{f_{p2}}{\sqrt{2}} \sqrt{1 + 4 \left( \frac{GB}{f_{p2}} \right)^2} - 1, \quad (4)$$

where  $GB = A_{ol} f_{p1}$ . Figure 2 illustrates in graphical form the dependence of the follower bandwidth on  $f_{p2}$ , both normalized by  $GB$ . Note that when  $f_{p2} \gg GB$ , then  $f_{-3dB} \approx GB$ ; otherwise,  $f_{-3dB} < GB$ , and  $f_{-3dB}$  decreases as  $f_{p2}$  decreases (for example, when the load capacitor  $C_L$  increases).

Despite the high accuracy and low output resistance of the buffer of Fig. 1(a), the maximum current that the circuit can deliver to the load is limited by the quiescent current  $I_B$  of the output stage, which limits positive slew rate to

$$SR_+ = \frac{I_{max}}{C_L + C_C} = \frac{I_B}{C_L + C_C}, \quad (5)$$

where  $C_L$  is the load capacitor. Hence, a large slew rate requires large quiescent power consumption. Note that (5) assumes that amplifier A has enough driving capability in order not to additionally limit slewing.

### 2. Proposed Class AB Two-Stage Unity-Gain Buffer

To avoid this drawback, the class AB topology of Fig. 1(b) can be derived which results from including a capacitor  $C_{bat}$  between nodes X and Y and a large resistive device  $R_{large}$  between node Y and the biasing voltage  $V_B$ . This modification makes the gate of  $M_2$  a quasi-floating node [9] with well

established DC voltage  $V_B$  but floating from a signal viewpoint. The static behavior of the circuit of Fig. 1(b) is identical to that of Fig. 1(a) since capacitance  $C_{\text{bat}}$  has no effect in quiescent conditions, and there is no voltage drop in resistance  $R_{\text{large}}$ . Hence, the quiescent current  $I_B$  in the output branch is accurately controlled as it is the result of mirroring the current in  $M_3$ , just as for the circuit of Fig. 1(a). If necessary, the quiescent current could be made very small to save static power because it does not limit slew rate in the class AB circuit of Fig. 1(b). A description follows. Assume that the input voltage  $V_{\text{in}}$  increases. For the output voltage to accurately track such variation as fast as possible, a large current must be delivered to the load. This large current can be delivered in Fig. 1(b) since an increase  $\Delta V_{\text{in}}$  at the input leads to a decrease  $-\Delta V_{\text{in}}$  at node X. Due to the large value of resistance  $R_{\text{large}}$  capacitor  $C_{\text{bat}}$  cannot discharge rapidly. Hence, this capacitor acts as a floating battery that translates this voltage decrease at node X to node Y, thus increasing the  $V_{\text{SG}}$  of  $M_2$  and providing the required output current. The decrease of voltage at node X also decreases the current in  $M_1$  below  $I_B$ , which also contributes to increasing the output current. Likewise, when input voltage decreases voltage at nodes X and Y increases, thus decreasing current in  $M_2$  and increasing current in  $M_1$  and resulting in a large current sunk from the load.

More specifically, RC high-pass filtering takes place between node X and node Y which is given by

$$\frac{V_Y(s)}{V_X(s)} = \alpha \frac{sR_{\text{large}}(C_{\text{bat}} + C_Y)}{sR_{\text{large}}(C_{\text{bat}} + C_Y) + 1}, \quad (6)$$

where  $\alpha = C_{\text{bat}}/(C_{\text{bat}} + C_Y)$ , and  $C_Y$  is the parasitic capacitance at node Y. Note that  $C_Y$  leads to attenuation  $\alpha$  from X to Y, which sets the minimum required value for  $C_{\text{bat}}$ . Capacitance  $C_Y$  is dominated by  $C_{\text{GS2}}$ . It is important to connect the top plate of  $C_{\text{bat}}$  to node Y instead of the bottom plate to minimize  $C_Y$ . The large resistance  $R_{\text{large}}$  does not need to have a precise value as long as it is high enough to provide a cutoff frequency  $1/[2\pi R_{\text{large}}(C_{\text{bat}} + C_Y)]$  lower than the minimum frequency component in node X to be transferred to node Y. Process, voltage, and temperature variations affecting the value of  $R_{\text{large}}$  are not relevant, and it can be implemented by a minimum-size diode-connected MOS transistor in a cutoff region or minimum-size transistor biased by another identical transistor in subthreshold region [12], leading to a compact and power-efficient implementation. Simulated values of  $R_{\text{large}}$  for this implementation range from 670 G $\Omega$  to 77 G $\Omega$  for a temperature interval from  $-40^\circ\text{C}$  to  $120^\circ\text{C}$ . The corresponding cutoff frequency ranges from 0.23 Hz to 2 Hz.

The only difference between the buffers of Fig. 1(a) and Fig. 1(b) in terms of small-signal operation is that  $M_2$  is just a biasing transistor in Fig. 1(a), but it contributes to the

transconductance gain of the output stage in Fig. 1(b). Hence, the small-signal expressions for the class A buffer in subsection II.1 apply by replacing  $g_{m1}$  by  $g_{m1} + \alpha g_{m2}$ . Thus, the low-frequency gain of the follower of Fig. 1(b) is given by (1), but here the loop gain increases to  $A_{ol} = G_{\text{mA}} R_A (g_{m1} + \alpha g_{m2})(r_{o1} \parallel r_{o2})$ .

The output resistance becomes

$$R_{\text{out}} = \frac{1}{G_{\text{mA}} R_A (g_{m1} + \alpha g_{m2})}. \quad (7)$$

The dominant pole  $f_{p1}$  and non-dominant pole  $f_{p2}$  become

$$f_{p1} \approx \frac{1}{2\pi R_A (g_{m1} + \alpha g_{m2})(r_{o1} \parallel r_{o2}) C_C}, \quad (8)$$

$$f_{p2} \approx \frac{g_{m1} + \alpha g_{m2}}{2\pi(C_X + C_L)},$$

where  $C_X$  now increases to

$$C_X \approx C_{\text{GS1}} + C_{\text{Cb}} + \frac{C_{\text{bat}} C_Y}{C_{\text{bat}} + C_Y}, \quad (9)$$

with  $C_{\text{Cb}}$  the bottom-plate to substrate capacitance of  $C_{\text{bat}}$ . Hence, the QFG technique increases the follower gain and decreases the output resistance and dominant pole frequency. Note, however, that the product  $GB = A_{ol} f_{p1}$  is the same as the class A follower. For  $C_L > C_X$ , the increase in  $C_X$  from (9) is not significant in (8) and the increase in the numerator of  $f_{p2}$  shifts  $f_{p2}$  to higher frequencies. From (4), this may slightly increase bandwidth of the class AB buffer versus its class A counterpart, as shown in Table 1. This increase is also observed in other QFG circuits [10].

Under quiescent conditions, current in  $M_2$  is  $I_2 = I_B$  and

$$V_{\text{SG2}} = V_{\text{SG2}}^Q = \sqrt{\frac{2I_B}{\beta_2}} + |V_{\text{TH2}}|, \quad (10)$$

where  $V_{\text{TH2}}$  and  $\beta_2 = \mu_n C_{\text{ox}}(W/L)_{M2}$  are the threshold voltage and transconductance factor, respectively, of transistor  $M_2$ , and superscript Q indicates quiescent value. When a positive input step  $V_{\text{step}}$  is applied to the buffer, voltage at node Y suddenly decreases by  $-\alpha A V_{\text{step}}$ , leading to a current in  $M_2$  which becomes larger than  $I_B$ :

$$I_2 = \frac{\beta_2}{2} \left( V_{\text{SG2}}^Q + \alpha A V_{\text{step}} - |V_{\text{TH2}}| \right)^2$$

$$= \frac{\beta_2}{2} \left( \sqrt{\frac{2I_B}{\beta_2}} + \alpha A V_{\text{step}} \right)^2. \quad (11)$$

Note from (11) that current  $I_2$  is not bounded by  $I_B$ , reflecting the class AB operation. For

$$V_{\text{step}} \gg \frac{1}{\alpha A} \sqrt{\frac{2I_B}{\beta_2}}, \quad (12)$$

the output current is  $I_{\text{out}} \approx I_2$  and  $SR_+$  becomes approximately



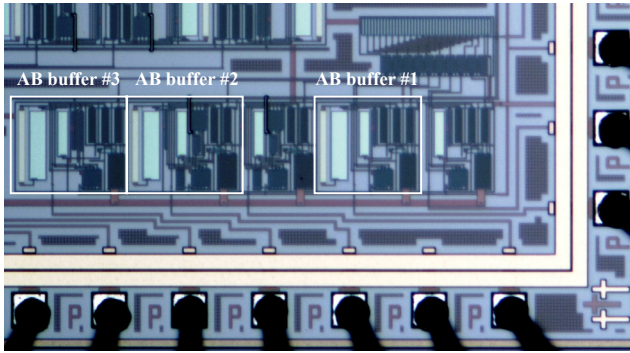


Fig. 4. Microphotograph of the fabricated chip.

using a 0.5  $\mu\text{m}$  CMOS n-well process with nominal nMOS and pMOS threshold voltages of 0.67 V and  $-0.96$  V, respectively. A microphotograph of the chip is shown in Fig. 4. Three buffers operate in class A, and they correspond to the circuit of Fig. 1(a) by replacing amplifier A by the three circuits of Fig. 3. The other three buffers operate in class AB and correspond to the replacement of amplifier A in Fig. 1(b) by the three topologies of Fig. 3. Supply voltage was set to  $\pm 1.65$  V, and the bias current was  $I_B = 10 \mu\text{A}$ . Transistor dimensions in  $\mu\text{m}/\mu\text{m}$  are 60/1 ( $M_1, M_8, M_9, M_{10}, M_{11}, M_{14}$ ), 100/0.6 ( $M_2, M_3, M_6, M_{6c}$ ), 200/0.6 ( $M_7, M_{7c}$ ), and 100/1 ( $M_4, M_5, M_{8c}, M_{9c}, M_{11c}, M_{12}$ ). An off-chip load capacitor of 22 pF was employed, which added to the pad and board parasitics leads an estimated load capacitance of about 30 pF. Capacitor  $C_{\text{bat}}$  was of 1 pF,  $C_C = 2$  pF, and  $R_{\text{large}}$  is a diode-connected PMOS of 1.5/0.6.

Figure 5 shows the measured harmonic distortion of the three fabricated class AB buffers following the approach of Fig. 1(b). Note that in all cases total harmonic distortion (THD) is below  $-60$  dB for input amplitudes of 1  $V_{\text{pp}}$  and below  $-50$  dB for input amplitudes of 2  $V_{\text{pp}}$ . Note also that distortion is dominated by the second-order harmonic. Therefore, a differential configuration would feature strongly reduced distortion levels dominated by the low third-order harmonic shown in the graphs of Fig. 5.

As expected, the lowest distortion for high input amplitudes corresponds to the buffer using the amplifier of Fig. 3(b), which is designed to tolerate the upper bias transistors to operate even in triode region. For low to medium input amplitudes, the buffer using the amplifier of Fig. 3(c) provides the best linearity, with  $\text{THD} < -70$  dB for  $V_{\text{in}} \leq 1.5 V_{\text{pp}}$ .

A comparison of the measured THD for the class A and class AB buffers of Fig. 1 is shown in Fig. 6. The upper graph compares the buffers using amplifier A of Fig. 3(a). The middle graph corresponds to the amplifier of Fig. 3(b). The lower one corresponds to that of Fig. 3(c). Note that although THD is similar for low input amplitudes, it strongly increases for the class A versions when input amplitude increases. This is due to slew-rate limitations of the class A buffers, which are unable to

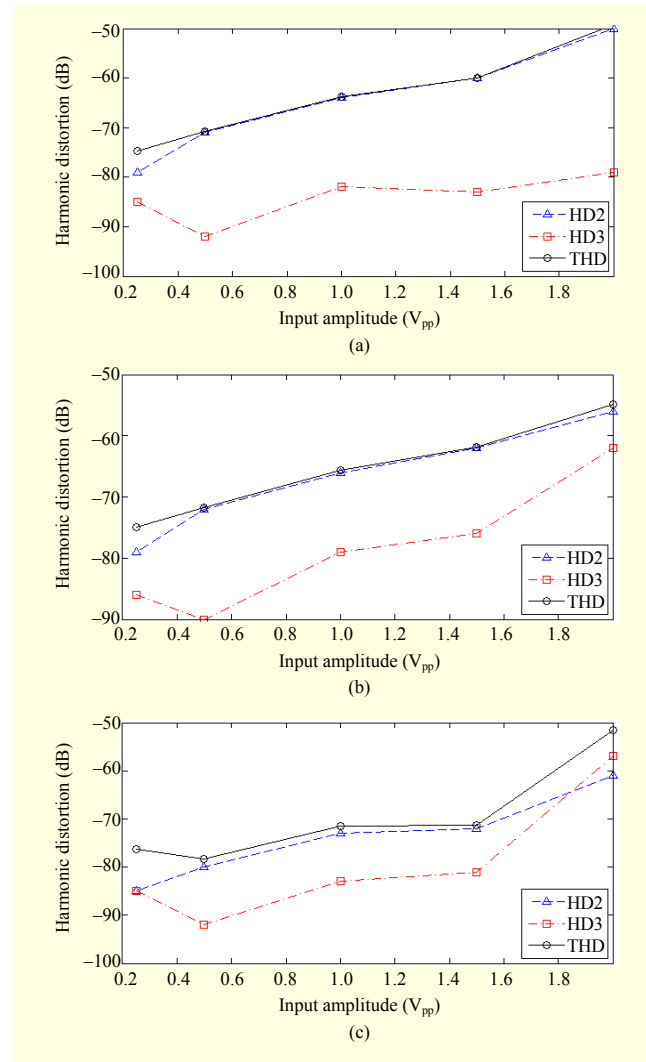


Fig. 5. Measured harmonic distortion at 100 kHz for different input amplitudes of three class AB buffers based on Fig. 1(b): (a) buffer using amplifier A of Fig. 3(a), (b) buffer using amplifier A of Fig. 3(b), and (c) buffer using amplifier A of Fig. 3(c).

track the rate at which input voltage increases for this load capacitance, strongly distorting the output waveform.

Figure 7 shows the measured response of the class A and AB buffers of Fig. 1 when an input square waveform of 100 kHz and 1.8  $V_{\text{pp}}$  is applied. The amplifier of Fig. 3(b) is used for both class A and class AB buffers. Note the increase in  $SR_+$ , which is 0.32  $\text{V}/\mu\text{s}$  for the class A buffer and 29  $\text{V}/\mu\text{s}$  for the class AB version. Similar results are obtained for the two other amplifiers of Fig. 3, which are not shown for brevity.

Table 1 summarizes the main performance parameters of the six fabricated buffers. Buffer class AB numbers 1, 2, or 3 correspond to the circuit of Fig. 1(b) with amplifier of Figs. 3(a) to (c), respectively. Similar notation is used for the class A buffers based on Fig. 1(a). Measurements in Table 1



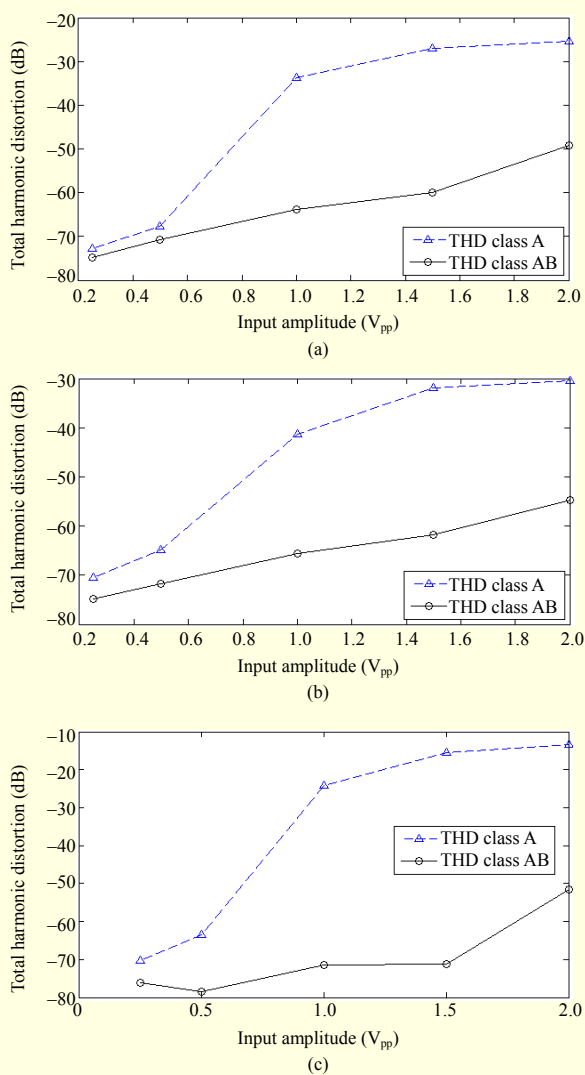


Fig. 6. Comparison of measured THD at 100 kHz for class A and class AB buffers of Fig. 1, using different input amplitudes: (a) buffers using amplifier A of Fig. 3(a), (b) buffers using amplifier A of Fig. 3(b), and (c) buffers using amplifier A of Fig. 3(c).

show that the class AB buffers improve slew rate by an approximate factor of 100, improve bandwidth by around 20%, and they do not degrade quiescent power or noise performance compared with the class A versions, but require only a modest increase in silicon area.

Comparison with some other class AB followers previously reported is shown in Table 2. Dynamic performance is difficult to compare since different loads and supply currents are used in different papers. To overcome this issue, Table 2 shows the current efficiency of the output stage ( $I_{\max}/I_{\text{bias}}$ ), that is, the ratio between the maximum output current  $I_{\max} \approx SR_+ \cdot C_L$  and the bias current  $I_{\text{bias}}$  of the output branch. It can be observed that the three class AB topologies presented here show higher current

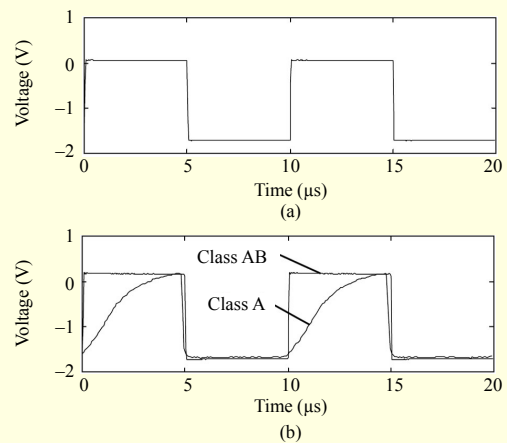


Fig. 7. Measured transient response of buffers in Fig. 1 using amplifier A of Fig. 3(b): (a) input waveform and (b) output waveforms of class A and class AB buffers.

Table 1. Measured performance of class A and class AB buffers.

	AB#1	A#1	AB#2	A#2	AB#3	A#3
SR <sub>+</sub> (V/μs)	25	0.27	29	0.32	20	0.21
THD@1V <sub>pp</sub> , 100 kHz (dB)	-63.8	-33.7	-74.3	-41.3	-71.5	-24.2
Input noise @50 kHz (nV/√Hz)	42	44	55	57	30	30
Quiescent power (μW)	198	198	198	198	165	165
BW (MHz)	12.2	10.4	13.4	11.9	8.4	5.8
Area (mm <sup>2</sup> )	0.014	0.011	0.017	0.015	0.025	0.021

efficiency driving the load than the other references in Table 2. Also in Table 2, the ratio between  $I_{\max}$  and the total quiescent current supplied  $I_{\text{supply}}$  is shown. The proposed buffers also compare favorably in terms of this ratio as well as in linearity and silicon area (considering the differences in feature size).

High-performance class AB buffers can be made featuring the high accuracy and dynamic range from class AB three-stage amplifiers [5]. The focus in this work is on micropower buffers for which having less stages is beneficial. However, the technique proposed could be expanded to three-stage implementations by using the idea of Fig. 1(b) at the output stage.

#### IV. Conclusion

A new and systematic way of designing class AB unity-gain buffers has been presented. The proposed method is based on using QFG transistors in the output stage of the general scheme

Table 2. Measured performance comparison with other class AB buffers.

	This work AB #1	This work AB #2	This work AB #3	Wong [1]	Kenney [7]	Lu [17]	Torralba [18]	Xing [19]	Lu [20]
CMOS tech.	0.5 $\mu\text{m}$	0.5 $\mu\text{m}$	0.5 $\mu\text{m}$	3 $\mu\text{m}$	2 $\mu\text{m}$	0.35 $\mu\text{m}$	0.5 $\mu\text{m}$	0.35 $\mu\text{m}$	0.35 $\mu\text{m}$
Supply volt.	$\pm 1.65$ V	$\pm 1.65$ V	$\pm 1.65$ V	$\pm 2.5$ V	5 V	3.3 V	1.5 V	3.3 V	3.3 V
Load capac.	30 pF	30 pF	30 pF	5 nF	20 pF	150 pF	18 pF	12 pF	150 pF
SR+	25 V/ $\mu\text{s}$	29 V/ $\mu\text{s}$	20 V/ $\mu\text{s}$	0.9 V/ $\mu\text{s}$	50 V/ $\mu\text{s}$	2.7 V/ $\mu\text{s}$	6.2 V/ $\mu\text{s}$	200 V/ $\mu\text{s}$	3.9 V/ $\mu\text{s}$
SR-	-27 V/ $\mu\text{s}$	-35 V/ $\mu\text{s}$	-17 V/ $\mu\text{s}$	-0.9 V/ $\mu\text{s}$	NA	-3.8 V/ $\mu\text{s}$	-14.5 V/ $\mu\text{s}$	NA	-2.7 V/ $\mu\text{s}$
$I_{\text{max}}/I_{\text{bias}}$	80	92.8	64	40	4.3	NA	3.7	4.8	NA
$I_{\text{max}}/I_{\text{supply}}$	13.3	15.4	10.7	15	3.8	1.8	1.9	2.4	2.7
THD	-63.8 dB (@1 V <sub>pp</sub> , 100 kHz)	-74.3 dB (@1 V <sub>pp</sub> , 100 kHz)	-71.5 dB (@1 V <sub>pp</sub> , 100 kHz)	-48 dB (@3.4 V <sub>pp</sub> , 100 kHz)	-60 dB (@1 V <sub>pp</sub> , 100 kHz)	-62.8 dB (@2.4 V <sub>pp</sub> , 20 kHz)	-50 dB (@0.6 V <sub>pp</sub> , 1 MHz)	-48 dB (@0.8 V <sub>pp</sub> , 700 kHz)	-64.5dB (@2 V <sub>pp</sub> , 20 kHz)
PSRR	56 dB	51 dB	53 dB	N.A	NA	NA	NA	>60 dB	NA
Input offset	8 mV	10 mV	5 mV	<10mV	NA	NA	NA	8.8 mV	NA
Input noise @50 kHz	42 nV/ $\sqrt{\text{Hz}}$	55 nV/ $\sqrt{\text{Hz}}$	30 nV/ $\sqrt{\text{Hz}}$	70 nV/ $\sqrt{\text{Hz}}$	NA	NA	NA	NA	NA
Quiescent power	198 $\mu\text{W}$	198 $\mu\text{W}$	165 $\mu\text{W}$	1.5 mW	1.3 mW	660 $\mu\text{W}$	90 $\mu\text{W}$	3.3 mW	714 $\mu\text{W}$
Bandwidth	12.2 MHz	13.4 MHz	8.4 MHz	6 MHz ( $C_L=0.1$ nF)	6 MHz	NA	NA	87 MHz	NA
Silicon area	0.014 mm <sup>2</sup>	0.017 mm <sup>2</sup>	0.025 mm <sup>2</sup>	0.645 mm <sup>2</sup>	NA	0.012 mm <sup>2</sup>	NA	0.010 mm <sup>2</sup>	0.087 mm <sup>2</sup>

of Fig. 1(a). Measurements demonstrate a notable improvement of dynamic performance with a minor penalty in terms of silicon area. The slew rate improvement factor is nearly 100. The resulting buffers can be applied in systems requiring accurate operation with very low quiescent power consumption.

## References

- [1] S.L. Wong and C.A.T. Salama, "An Efficient CMOS Buffer for Driving Large Capacitive Loads," *IEEE J. Solid State Circuits*, vol. 21, no. 3, June 1986, pp. 464-469.
- [2] F. You, S.H.K. Embabi, and E. Sanchez-Sinencio "Low-Voltage Class AB Buffers with Quiescent Current Control," *IEEE J. Solid State Circuits*, vol. 33, no. 6, June 1998, pp. 915-920.
- [3] R. van Dongen and V. Rikkink, "A 1.5 V class AB CMOS Buffer Amplifier for Driving Low-Resistance Loads," *IEEE J. Solid-State Circuits*, vol. 30, no. 12, Dec. 1995, pp. 1333-1338.
- [4] M.D. Pardo and M.G. Degrauwe, "A Rail-to-Rail Input/Output CMOS Power Amplifier," *IEEE J. Solid-State Circuits*, vol. 25, no. 2, Apr. 1990, pp. 501-504.
- [5] F. Op't Eynde et al., "A CMOS Large Swing Low-Distortion Three-Stage Class AB Power Amplifier," *IEEE J. Solid-State Circuits*, vol. 25, Feb. 1990, pp. 265-273.
- [6] A. Torralba et al, "Compact Low-Voltage Class-AB Analogue Buffer," *Electron. Lett.*, vol. 42, no. 3, Feb. 2006, pp. 152-154.
- [7] J.G. Kenney et al., "An Enhanced Slew Rate Source Follower," *IEEE J. Solid State Cir.*, vol. 30, no. 2, Feb. 1995, pp. 144-146.
- [8] J. Ramirez-Angulo et al., "A New Family of Very Low-Voltage Analog Circuits Based on Quasi-Floating-Gate Transistors," *IEEE Trans. Cir. Syst. II*, vol. 50, no. 5, May 2003, pp. 214-220.
- [9] J. Ramirez-Angulo et al., "Very Low-Voltage Analog Signal Processing Based on Quasi-Floating Gate Transistors," *IEEE J. Solid State Cir.*, vol. 39, no. 3, Mar. 2004, pp. 434-442.
- [10] J. Ramirez-Angulo et al., "A Free but Efficient Low-Voltage Class AB Two-Stage Operational Amplifier," *IEEE Trans. Circuits Syst. II*, vol. 53, no. 7, July 2006, pp. 568-571.
- [11] J. Ramirez-Angulo et al., "Class-AB Fully Differential Voltage Followers," *IEEE Trans. Circuits Syst. II*, vol. 55, no. 2, Feb. 2008, pp. 131-135.
- [12] M. Bikumandla et al., "Biasing CMOS Amplifiers Using MOS Transistors in Subthreshold Region," *IEICE Electron. Expr.*, vol. 1, no. 12, Sept. 2004, pp. 339-345.
- [13] A.J. Lopez-Martin et al., "Power-Efficient Class AB CMOS Buffer," *Electron. Lett.*, vol. 45, no. 2, Jan. 2009, pp. 89-90.
- [14] Y. Haga and I. Kale, "Class AB Rail-to-Rail CMOS Buffer with Bulk-Driven Super Followers," *Proc. European Conf. Circuit Theory and Design*, Antalya, Turkey, 2009, pp. 695-698.

- [15] J. Ramirez-Angulo et al., "Low Voltage Differential Input Stage with Improved CMRR and True Rail-to-Rail Common-Mode Input Range," *IEEE Trans. Circuits Syst. II*, vol. 55, no. 12, Dec. 2008, pp. 1229-1233.
- [16] A.J. Lopez-Martin et al., "Low-Voltage Super Class AB CMOS OTA Cells with Very High Slew Rate and Power Efficiency," *IEEE J. Solid-State Circuits*, vol. 40, no. 5, May 2005, pp. 1068-1077.
- [17] C.-W. Lu, Y.-C. Shen, and M.-L. Sheu, "A High-Driving Class-AB Buffer Amplifier with a New Pseudo Source Follower," *Proc. IFIP Int. Conf. VLSI*, Atlanta, USA, Oct. 2007, pp. 105-109.
- [18] A. Torralba et al., "Compact Low-Voltage Class AB Analogue Buffer," *Electron. Lett.*, vol. 42, no. 3, Feb. 2006, pp. 152-154.
- [19] G. Xing, S.H. Lewis, and T.R. Viswanathan, "Self-Biased Unity-Gain Buffers with Low Gain Error," *IEEE Trans. Circuits Syst. II*, vol. 56, no. 1, Jan. 2009, pp. 36-40.
- [20] C.-W. Lu and K.-J. Hsu, "A Large-Swing High-Driving Low-Power Class-AB Buffer Amplifier Employing Adaptive-Gain Error Amplifiers," *Proc. 6th Int. Conf. Devices Circuits Syst.*, Playa del Carmen, Mexico, Apr. 2006, pp. 243-246.



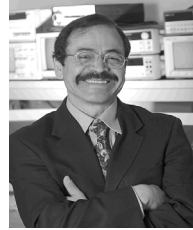
**Antonio Lopez Martin** is a professor with the Public University of Navarra and an adjunct professor with the New Mexico State University. His current research interests include wireless transceivers and sensor interfaces. He has published more than 300 technical contributions in books, journals, and conferences. He holds 6 patents. Dr. Lopez was an associate editor of the IEEE Transactions and Circuits on Systems-I (2006 to 2007) and II (2008 to 2009). His recent awards include the ANIT's Engineer of the Year Award, the Caja Navarra Research Award, the Young Investigator Award from the Complutense University of Madrid, the 2005 IEEE Transactions on Education Best Paper Award, and the European Center of Industry and Innovation Award for excellence in transfer of research results to industry.



**Jose Maria Algueta Miguel** received the BS in telecommunications engineering from the Public University of Navarra, Spain, in 2008. Currently, he is an assistant researcher working toward the PhD with the same university. His research interests include low-voltage continuous-time filter design.



**Lucia Acosta** received the BS and PhD in telecommunications engineering from the University of Sevilla, Spain, in 2005 and 2010, respectively. She has been an invited researcher with New Mexico State University, Las Cruces, NM, in 2007 and 2008. Currently, she is a researcher with the Public University of Navarra, Spain. Her research interests are related to low-voltage low-power analog circuit design.



**Jaime Ramirez-Angulo** is currently a Klipsch Distinguished Professor, IEEE fellow, and Director of the Mixed-Signal VLSI lab at the Klipsch School of Electrical and Computer Engineering, New Mexico State University (Las Cruces, New Mexico), USA. He received a degree in communications and electronic engineering (professional degree), an MSEE from the National Polytechnic Institute in Mexico City, and a Dr.-Ing from the University of Stuttgart in Stuttgart, Germany, in 1974, 1976, and 1982, respectively. He was a professor at the National Institute for Astrophysics Optics and Electronics (INAOE) and at Texas A&M University. His research is related to various aspects of design and testing of analog and mixed-signal Very Large Scale Integrated Circuits.



**Ramón Gonzalez Carvajal** received the BS and PhD (honors) in electrical engineering from the University of Seville, Seville, Spain, in 1995 and 1999, respectively. Since 1996, he has been with the Department of Electronic Engineering, School of Engineering, University of Seville, where he has been an associate professor (1996), and a professor (2002). He was an invited researcher at the Klipsch School of Electrical Engineering, NMSU, in the summers of 1999 and 2001 to 2004, and also at the Electrical Engineering Department of Texas A&M University in 1997. Dr. Carvajal also holds the position of adjunct professor at the Klipsch School of Electrical Eng., NMSU. Dr. Carvajal has published more than 60 papers in international journals and more than 130 in international conferences. His research interests are related to low-voltage low-power analog circuit design, A/D and D/A conversion, and analog and mixed-signal processing.